ACS APPLIED MATERIALS & INTERFACES

Research Article

www.acsami.org

An Electrochemical Impedance Spectroscopy Investigation of the Overpotentials in Li–O_2 Batteries

Jonathan Højberg,*[,†,‡,§] Bryan D. McCloskey,[†,⊥] Johan Hjelm,[‡] Tejs Vegge,[‡] Keld Johansen,[§] Poul Norby,[‡] and Alan C. Luntz[†,∥]

[†]IBM Almaden Research Center, San Jose, California 95120, United States

[‡]DTU Energy, Frederiksborgvej 399, DK-4000 Roskilde, Denmark

[§]Haldor Topsøe A/S, Nymøllevej 55, DK-2800 Kgs. Lyngby, Denmark

[∥]SUNCAT, SLAC National Accelerator Laboratory, Menlo Park, California 94025, United States

Supporting Information

ABSTRACT: Lithium–O_2 (Li–O_2) batteries are currently limited by a large charge overpotential at practically relevant current densities, and the origin of this overpotential has been heavily debated in the literature. This paper presents a series of electrochemical impedance measurements suggesting that the increase in charge potential is not caused by an increase in the internal resistance. It is proposed that the potential shift is instead dictated by a mixed potential of parasitic reactions and Li_2O_2 oxidation. The measurements also confirm that the rapid potential loss near the end of discharge ("sudden death") is explained by an increase in the charge transport resistance. The findings confirm that our theory and conclusions in ref 1, based on experiments on smooth small-area glassy carbon cathodes, are equally valid in real Li–O_2 batteries with porous cathodes. The parameter variations performed in this paper are used to develop the understanding of the electrochemical impedance, which will be important for further improvement of the Li–air battery.

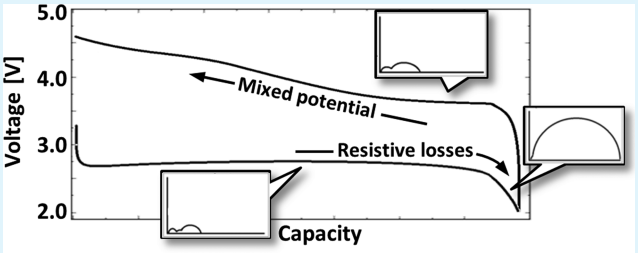

KEYWORDS: *Li–O_2 batteries, electrochemical impedance spectroscopy, overpotential, mixed potential, battery performance*

1. INTRODUCTION

Lithium–air and Li–O_2 batteries have attracted much attention in recent years because of a potentially high specific energy density and low cost. Furthermore, the fundamental electrochemistry has very low reaction barriers, which, in principle, enables a high cycle efficiency. The low reaction barriers have been predicted by Hummelshøj et al.[2,3] using density functional theory (DFT) and proven recently by Viswanathan et al.[4] using experiments on flat glassy carbon cathodes in an electrolysis cell.

However, more realistic batteries with porous electrodes show large overpotentials,[5] which significantly reduces the cycle efficiency. Understanding this is crucial to develop a commercially viable Li–O_2 technology. The origin of the overpotential has been investigated intensively. We have previously used DFT modeling,[2,4] differential electrochemical mass spectrometry (DEMS), and Li_2O_2 titration.[5] In addition to this, and among others, Zhong et al. used in situ transmission electron microscopy (TEM) to study growth mechanisms,[6] and Chen et al. used a redox-mediator to investigate limitations in the electronic conductivity.[7]

In this study, we use electrochemical impedance spectroscopy (EIS) that is often used as a diagnostic tool to identify the underlying mechanisms of the polarization curves in electrochemical systems such as lithium-ion batteries and fuel cells, as it is a powerful tool to obtain noninvasive in situ information on degradation mechanisms and possible bottlenecks in the electrochemical reactions. Very recently, Adams et al. and Landa-Medrano et al. have also used EIS to measure the internal resistances of a Li–O_2 battery using a two-electrode configuration.[8,9] They varied parameters like cathode morphology, oxygen partial pressure, salt concentration, and state-of-charge (SOC), and they succeed in assigning the different impedance contributions to the processes of either the anode or the cathode. The batteries investigated were, however, not characterized by DEMS and Li_2O_2 titration, which are important complementary methods necessary to link EIS results to the fundamental electrochemistry.

In this work, we used an intensely studied and well-characterized in-house reference system used in a number of previous publications.[5,10−15] It consists of an XC-72 carbon black and poly(tetrafluoroethylene) (PTFE) binder cathode, lithium metal anode, and 1 M LiTFSI/1,2-dimethoxyethane electrolyte. A series of electrochemical impedance spectra was measured at different state-of-discharge (SOD), SOC, and at different current densities with a focus on three states of the

Received: November 6, 2014
Accepted: January 27, 2015
Published: January 27, 2015

DOI: 10.1021/am5083254
ACS Appl. Mater. Interfaces 2015, 7, 4039−4047

Li−O_2 battery electrochemistry: the discharge plateau, sudden death at the end of discharge, and the initial stage of the charging process.

By combining the measurements with previous results presented by McCloskey and Luntz et al.,[1,4,5] the EIS measurements are related to the measured potential.

We show that the overpotential during discharge is caused by internal resistance and is dominated by the charge transport through the deposited Li_2O_2 at the end of discharge. During charge, however, the potential increase reflects a mixed potential of parasitic reactions and Li_2O_2 oxidation.

2. EXPERIMENTAL SECTION

Most of the experimental setup and procedures have been described in detail previously in ref 11 and are only briefly described here. The cathodes were prepared by air-spraying a carbon/PTFE dispersion onto a 316SS 100 mesh (TWP, Inc., Berkeley, CA). The slurries were prepared by sonicating a carbon black powder (Vulcan XC72, www.fuelcellstore.com) and PTFE (60 wt % dispersion in water, Sigma-Aldrich) in a 3:1 wt/wt ratio in a 20:80 isopropanol/water mixture. A Badger model 350 air sprayer was used to uniformly coat the SS mesh (the SS mesh was rinsed in acetone several times prior to cathode preparation). Prior to cutting 12 mm diameter cathodes from the carbon-coated SS mesh, the mesh was allowed to air-dry for 1 h. All cathodes were dried in vacuum at 120 °C for at least 12 h, washed in pure 1,2-dimethoxyethane (DME) in a glovebox, followed by a second drying under vacuum for 10 min, and then at 200 °C in the glovebox for at least 1 h. A typical carbon loading was two milligrams per cathode.

All solvents and salts in this study were purchased from Novolyte (Purolyte electrolyte grade), stored in an argon glovebox (0.1 ppm of O_2 and H_2O) and used without further purification. The H_2O content of solvents was periodically checked with a Karl Fischer titrator (Metrohm Inc.) and found to be no more than 20 ppm. The measurements were made with an 11 mm diameter lithium metal anode, a 12.5 mm diameter Celgard 2500 separator, a 12 mm diameter cathode, and 60 μL of 1 M bis(trifluoromethane)sulfonimide lithium salt (LiTFSI) dissolved in DME.

The test cell used in this study is shown in Figure S1 in the Supporting Information. The cell components were stacked between SS alloy 20 anode and cathode tips that were hermetically sealed against a quartz tube using compressed Markez O-rings (Marco Rubber). Capillaries were silver soldered into the cathode tip to allow gases to be fed to and swept away from the cell. Gases swept away from the cell could be quantitatively identified using the DEMS setup described in detail in ref 10.

2.1. Electrochemical Impedance Spectroscopy. All electrochemical measurements were made with a BioLogic VMP3 potentiostat. Electrochemical impedance spectra were measured while a current was drawn (GEIS) to investigate the processes under relevant conditions as discussed previously by Adams et al.[8] Impedance was measured at currents between 15 μA (13 μA/cm^2) and 1 mA (0.88 mA/cm^2). Frequencies between 4 mHz and 100 kHz were investigated with 15 points per decade and an alternating current (AC) amplitude of 10% of the direct current (DC) level. This typically gave an AC potential response amplitude of 2−5 mV, which was found to be within the linear regime, while still ensuring a sufficient signal-to-noise ratio.

To distinguish impedance contributions from the anode and the cathode in a two-electrode cell, it is often necessary to vary physical parameters that will affect the two electrodes differently. We used three methods: (i) measuring impedance at open-circuit voltage (OCV) in argon atmosphere to prevent the oxygen reduction/oxidation, (ii) using a symmetrical cell of two predischarged cathodes, and (iii) testing a different cathode (see Figure 4 below and Figures S2 and S3 in the Supporting Information). In the symmetrical cell, the anode/cathode reactions are oxidation/reduction of Li_2O_2, which remove any lithium metal-related contributions from the EIS measurement. Both cathodes in the symmetrical cell initially discharged 0.25 mAh in separate cells before they were combined in a new cell. The cathodes were rinsed with DME after the individual discharge to remove the electrolyte salt before the cathodes were used in the symmetrical cell. The symmetrical cell was tested in O_2 gas and was made without exposing the cathodes to air at any point.

2.2. Modeling Li−O_2 Impedance. The impedance is defined as the derivative of the *iv* curve:

$$Z(i) = \frac{\partial v}{\partial i} = \frac{\partial \eta}{\partial i} \tag{1}$$

where v is the potential, i is the current density, and η is the overpotential. Therefore, the impedance is linked closely to the Tafel plot, which has previously been used to describe reaction mechanisms in Li−O_2 batteries.[4,10,16,17] From the Tafel equation, the overpotential is seen to be proportional to $\log(i)$ at large overpotentials ($|\eta| \gg RT/nF$), but as our batteries contain a porous cathode, this ideal behavior is not applicable. The consequences of a porous electrode have been investigated by Lasia and show that the Tafel slope will increase at higher currents.[18] This is in line with our measurements as well as previous Li−O_2 battery measurements by Viswanathan et al. and Adams et al. on porous electrodes.[4,8] To describe the measurements better

$$\eta = |v - \mathrm{OCV}| = c_1 \cdot i^{c_2} \tag{2}$$

is applied as an empirical model, when eq 1 is used to compare the measured impedance with the overpotential. OCV is the open circuit potential, and c_1 and c_2 are constants. As c_2 is found to be less than 1 in Section 3.4, $Z(i)$ is expected to be larger at small currents according to eq 1.

The measured impedance response can, to a first approximation, be described using an equivalent circuit model consisting of three Voigt elements (parallel connected resistor with a constant phase element (CPE)) connected in series, see Figure S4a in the Supporting Information. The impedance of the Voigt elements is adopted from Hirschorn et al.,[19] and the total impedance, $Z(\omega)$, is thus given by

$$Z(\omega) = R_s + \sum_{i=1,2,3} \frac{R_i}{1 + (j\omega)^{n_i} Q_i R_i} \tag{3}$$

where ω is the angular frequency, and R_i, Q_i, and n_i are parameters in Voigt element i. Even though the model is not anchored in an electrochemical model, it is likely that key physical processes like charge transfer reactions, diffusion, and electronic transport through the Li_2O_2 layer will dominate one or more of the observed features in the spectra. Therefore, parametrization using the simplified model makes it possible to determine the magnitude of these processes, although each feature may contain contributions from multiple physical

DOI: 10.1021/am5083254
ACS Appl. Mater. Interfaces 2015, 7, 4039−4047

processes, and anode and cathode processes may overlap to some extent. The sum of the frequency-dependent resistances R_1, R_2, and R_3 is the polarization resistance, R_p. The equivalent circuit fits are made using the scipy optimizer fmin_slsqp using the software package RAVDAV 0.9.7.[20]

The Voigt elements have three parameters: R, Q, and n. R is the DC resistance, and Q and n are parameters of the CPE. If $n = 1$, the CPE is a capacitor, and even if n is between 0.7 and 1, a pseudocapacitance, C^*, can be calculated. This criterion is met in all measurements presented in this work, except for the very end of the 20 μA discharge presented in Figure 3. As discussed in detail by Jamnik et al.,[21] this capacitance is typically a double-layer capacitance related to the process, and by comparing with reference values, it is possible to estimate the surface area contributing to the process. This can be used to distinguish reactions at the flat lithium anode from reactions in the porous cathode, since the surface areas of these are ~1 cm^2 and 1 m^2, respectively. The capacitance at the lithium metal surface in an organic electrolyte is typically 10–20 μF/cm^2 as reported by Aurbach et al.,[22,23] and the capacitance of XC72 is 12.6 F/g in an organic aprotic electrolyte as reported by Barbieri et al.[24] From this, it is calculated that the capacitances should be in the range of 10 μF and 25 mF for the anode and cathode, respectively. These values should then be compared with the pseudocapacitance, calculated from the equivalent circuit parameters according to Hirschorn et al.[19]

$$C^* = Q^{1/n}\left(\frac{R_\Omega R}{R_\Omega + R}\right)^{(1-n)/n} \quad (4)$$

where R, Q, and n are fitting parameters from the Voigt elements, and R_Ω is the DC resistance at the investigated frequency. As discussed by Zoltowski et al., the pseudocapacitance of a CPE element is not well-defined,[25] which means that the surface area obtained using C^* might vary slightly from the actual surface area, but the order of magnitude and relative changes are still valid.

The capacitance is expected to change during discharge as the dielectric Li_2O_2 is deposited. The relative permittivity ε_r of Li_2O_2 has been measured to be 30–35 by Gerbig et al. and Dunst et al.[26,27] Using a value of 30 to calculate the capacitance of the Li_2O_2 layer in series with a typical electrode–electrolyte capacitance of 20 mF, a Li_2O_2 layer of 8 nm will halve the cathode capacitance. A similar calculation can be made for the Li_2CO_3 interface layer between the cathode and the Li_2O_2. Using the relative permittivity of Li_2CO_3 of 4.9 measured by Young et al.,[28] the capacitance will be halved with a layer thickness of 1 nm.

The role of oxygen diffusion in the electrolyte has been discussed in several papers.[29−31] To evaluate the significance of diffusion, the Damköhler number, Da, can be used as a quick comparison between the oxygen consumption/evolution with the diffusion rate.[29] Using typical values for our system, Da is 0.3 at a current of 250 μA, which means that the diffusion rate is ~3 times higher than the consumption rate. Oxygen diffusion is therefore not expected to be dominating, but it will have some significance.

Basic requirements for carrying out EIS measurements are that the system is stable, causal, and linear. Among other things, this implies that no (or only a negligible) change in voltage and impedance characteristics is allowed during the measurement period. Methods have been proposed to deal with impedance measurements in nonstationary systems such as a PEM fuel cell with hindered water removal during operation.[32] This approach, however, requires interpolation, which is difficult to apply in this case with a dramatically decreasing cell voltage toward the end of discharge of the battery. Without use of such methods, one can reduce drift problems by decreasing the measurement time or decreasing the change of the system. To do this, we optimized the frequency range and compared impedance spectra from stable low-current measurements (18 μA/cm^2 cathode) with impedance spectra from measurements at less stable but more realistic current densities (>0.2 mA/cm^2 cathode).

The Kramers–Kronig relation was used to evaluate the causality of all measurements. The largest deviations occur at low frequencies as the electrochemistry changes during the measurement. To minimize this effect, a frequency cutoff level of 5% deviation of the Kramer–Kronig transform was used.

3. RESULTS

All measurements were performed using a system with an XC72 carbon black cathode, DME/LiTFSI electrolyte, and lithium anode. This system has been characterized extensively in previous publications from 2011 to 2013 by McCloskey et al.[5,10−15] The most important methods used in these studies are differential electrochemical mass spectrometry (DEMS), peroxide titration, and X-ray diffraction.

In this work, we used DEMS to quantify gas consumption and release during discharge and charge at all investigated current densities to verify that the measured impedance can be related to previous work. A ratio of 2.0 e^-/O_2 was observed during discharge at all investigated currents between 10 μA (8.8 μA/cm^2) and 5 mA (4.4 mA/cm^2). During charge, the amount of oxygen released corresponded to 2.5 e^-/O_2 until a potential of 3.7 V. Above this potential, the ratio changed to 3 e^-/O_2. CO_2 was evolved at potentials above 4.2 V.

The OCV was measured as a function of discharge and charge to ensure an accurate determination of the overpotential. A full discharge–charge cycle at 250 μA (220 μA/cm^2) is seen in Figure 1. The battery was allowed to relax to

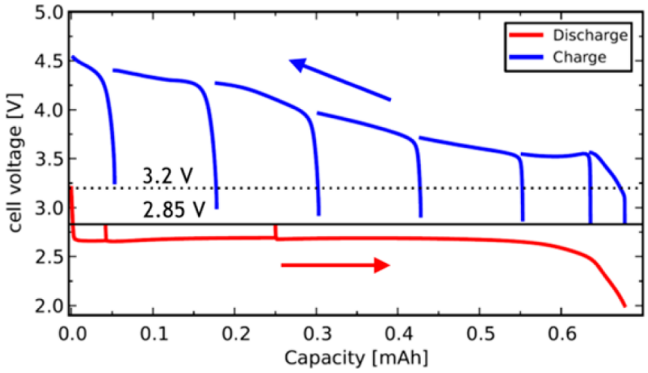

Figure 1. Measurement of OCV through a 250 μA (220 μA/cm2) discharge and charge. The steep voltage transients occur when the battery is allowed to relax at OCV.

OCV by interruption of the current a number of times during both discharge and charge, which is seen as steep voltage transients in Figure 1. The relaxation criteria were a change in cell voltage of less than 1 mV/h or a relaxation time of 15 h. The initial OCV was 3.2 V. The OCV decreased to 2.85 V after a short period of discharge and stayed at this value during the entire discharge—also after reaching the 2.0 V cutoff at sudden

DOI: 10.1021/am5083254
ACS Appl. Mater. Interfaces 2015, 7, 4039–4047

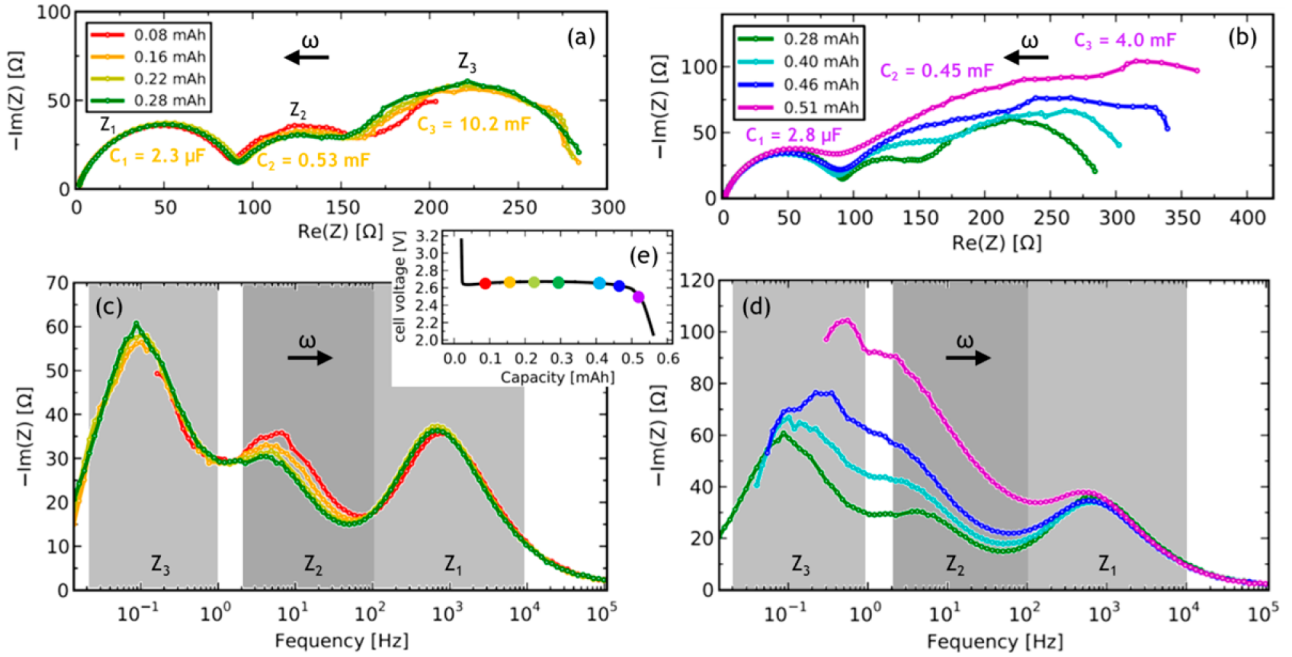

Figure 2. Nyquist plot (a) and (b) and Bode-like plot (c) and (d) of impedance measurements during a 250 μA (220 μA/cm2) constant current discharge. The approximate SODs are shown in (e) and in the legends of (a) and (b). Three processes are identified and named Z_1, Z_2, and Z_3, and the corresponding peak frequencies are within the gray intervals marked in (c) and (d) at all current densities and SODs investigated.

Table 1. Peak Frequencies, Resistances, and Pseudocapacitances from Selected Impedance Fit[a]

	f_1 [Hz]	f_2 [Hz]	f_3 [Hz]	R_1 [Ω]	R_2 [Ω]	R_3 [Ω]	C_1^* [mF]	C_2^* [mF]	C_3^* [mF]
discharge at 250 μA									
0.16 mAh	733	5.4	93×10^{-3}	96	56	145	2.3×10^{-3}	0.53	10.2
0.51 mAh	605	3.4	184×10^{-3}	94	92	188	2.8×10^{-3}	0.45	4.0
discharge at 20 μA									
0.5 mAh	470	1.15	5.5×10^{-3}	109	50	1007	3.1×10^{-3}	2.8	19.3
1.9 mAh	464	1.12	9.9×10^{-3}	107	158	2131	3.2×10^{-3}	0.6	2.0
2.3 mAh	479		1.1×10^{-3}	114		14 097	2.9×10^{-3}		0.8
charge at 250 μA									
0.03 mAh	678	9.6	267×10^{-3}	65	166	497	3.6×10^{-3}	76×10^{-3}	1.0
0.42 mAh	983	14.0	19×10^{-3}	255	105	700	0.6×10^{-3}	99×10^{-3}	9.0

[a]The expected capacitances for the full anode and cathode are 10 μF and 25 mF, respectively. Typical values of n are $n_1 = 0.77$, $n_2 = 0.86$, and $n_3 = 0.78$.

death. During charge, the OCV was 2.85 V, but it increased slightly toward the end of charge where it reached 3.2 V.

3.1. Discharge to Sudden Death at 250 μA. EIS measurements from the first discharge at 250 μA (220 μ/cm^2) are shown in Figure 2a–d. The spectra were measured while drawing a current, which means that the SODs shown in Figure 2 and Table 1 are approximate values. Three arcs are distinguished in the Nyquist plot in Figure 2a. They were almost constant in the first part of the discharge but changed as the potential decreased near the end of discharge. The three identified impedance contributions are labeled Z_1, Z_2, and Z_3, and, on the basis of a fit to the equivalent circuit given in eq 3 and shown in Figure S4a in the Supporting Information, the corresponding peak frequencies, resistances, and pseudocapacitances are calculated. The values from two of these calculations are given in Table 1.

It is seen that R_1 is constant through the discharge, whereas R_2 and R_3 increase and C_3^* decreases. The decrease of C_3^* and increase of R_3 through the discharge could be a blocking of the cathode surface. The magnitudes of the pseudocapacitances indicate that Z_1 originates from an anode process, and Z_2 and Z_3 originate from cathode processes. The cathode blocking and identification of reaction processes in the impedance spectra are discussed further in Section 4.1.

The peak frequencies changed between different current densities and close to sudden death. In all of our measurements, however, f_1 was between 100 Hz and 10 kHz, f_2 was between 2 and 100 Hz, and f_3 was between 20 mHz and 1 Hz. These intervals are shown in Figure 2c,d, and the clear separation helps in identifying the different impedance contributions.

3.2. Discharge to Sudden Death at 20 μA. We decreased the discharge current to 20 μA (18 μA/cm^2) to increase the stability of the system during the impedance measurements, see Figure 3. When comparing this with the previous discharge at 250 μA presented in Figure 2, it is important to note that both the capacity and the polarization resistance, R_p, are significantly larger in the 20 μA discharge.

On the basis of a fit using eq 3, representing the equivalent circuit presented in Figure S4a in the Supporting Information, the resistance and pseudocapacitance parameters of Z_1, Z_2, and

DOI: 10.1021/am5083254
ACS Appl. Mater. Interfaces 2015, 7, 4039–4047

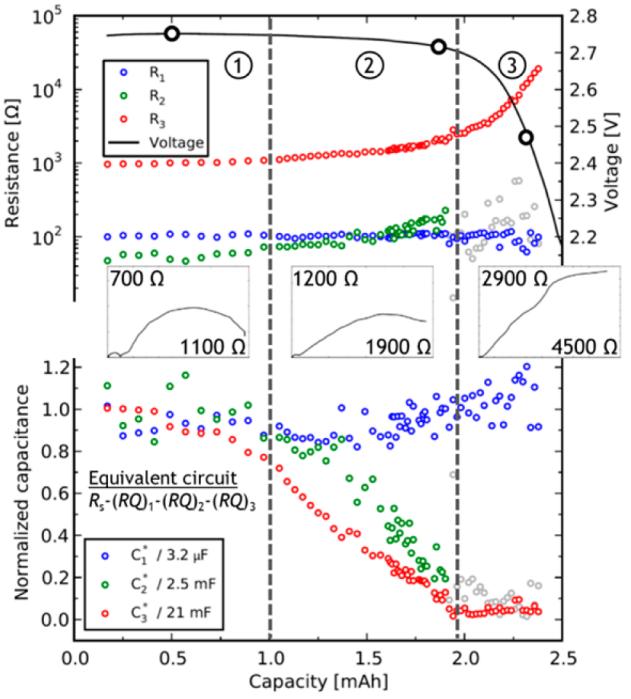

Figure 3. Resistances and normalized pseudocapacitances determined from EIS measurements in a 20 μA (18 μA/cm2) constant current discharge to 2.2 V using eq 3. Nyquist plots are shown at three representative stages, and the corresponding SODs are marked with circles on the voltage profile. R_2 and C_2^* could not be determined well at the end of discharge and are thus greyed out.

Z_3 are presented in Figure 3 and summarized in Table 1. The parameters of Z_1 were constant through the entire discharge, and the change of parameters related to Z_2 and Z_3 are divided into three parts as indicated in Figure 3: (1) At 0−40% SOD, only negligible change was observed, (2) at 40−80% SOD, R_2 and R_3 increased 2−3 times, and C_2^* and C_3^* decreased by 95%, and (3) at 80−100% SOD, R_3 increased exponentially to 14.1 kΩ at 90% SOD (more than 10 times the initial value), the pseudocapacitances stayed at ∼5% of the initial value, and the voltage dropped. Parameters related to Z_2 could not be determined in the last part of the discharge because of an overlap with Z_3.

At 20 μA, the average relative Kramers−Kronig deviation at frequencies from 1 mHz to 10 Hz was typically 0.5% at the plateau, increasing near sudden death to 2% at 2.2 V. The n_3 value got below 0.7 in the end of the discharge to typical values of 0.62. This means that the pseudocapacitance C_3^* is less meaningful to calculate.

3.3. EIS Measurement in Argon. A potentiostatic EIS measurement at OCV with 5 mV amplitude was made on a fresh battery in argon atmosphere before exposure to oxygen to investigate reactions not related to oxygen reduction. The measurement is shown in Figure 4, and clearly, reactions were still taking place in the absence of oxygen, as Z_1 and Z_2 were still present. The low frequency tail could be modeled with a capacitor, C_3, which means that no charge transfer reaction is present for this process. The spectrum was modeled with the equivalent circuit *R-RQ-RQ-RQ-C*, shown in Figure S4c in the Supporting Information. The capacitance C_3 was 18.3 mF, and the pseudocapacitances C_1^* and C_2^* were 1.2 μF and 0.2 mF, respectively. The presence of Z_2 suggests that this process is not related to oxygen reduction.

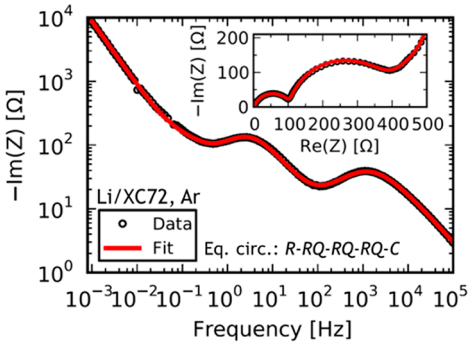

Figure 4. Bode plot and Nyquist plot (inset) of a potentiostatic EIS measurement at OCV in argon atmosphere. The spectrum is modeled with an *R-RQ-RQ-RQ-C* circuit, shown in Figure S4c in the Supporting Information.

3.4. *iv* Curve at the Discharge Plateau. As discussed in Section 2.2, the impedance is the slope of the *iv*-curve at a given current. To obtain a full understanding of the relationship between the impedance and the overpotential, it is necessary to investigate the current dependence of the impedance. We did this by measuring the impedance at the plateau at ∼40% of the total capacity at different current densities and compared this with the corresponding *iv* curve. As the impedance is almost constant in the first part of a discharge, the exact time of measurement was of less importance. To avoid effects of degradation in the battery, each point in the plot was made with a fresh battery. To eliminate variations due to different masses of the cathodes, both currents and impedances were weighed with the mass of carbon.

Figure 5 shows the *iv* curve of the plateau potential as a function of current density (red dots). The values are fitted

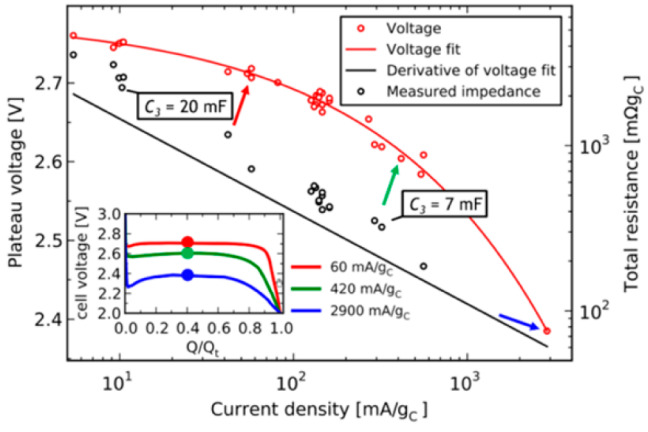

Figure 5. Plateau voltage dependence on current density (red dots) from 10 μA (9 μA/cm2) to 5 mA (4.4 mA/cm2). Equation 2 is fitted to the data (red line), which is then differentiated (black line) and compared with the total resistance (black dots) measured with impedance. Three representative discharge curves show how the plateau voltage is determined. The impedance and current density were weighed by the carbon mass of each electrode.

with eq 2 (red line) with OCV, c_1, and c_2 as fitting parameters. The result is OCV = 2.78 V, c_1 = 12 mV·$(g_C/mA)^{0.44}$ and c_2 = 0.44, which correspond to a Tafel slope of 120 millivolts per decade at 180 mA/g_C. This is in line with previous publications by Viswanathan et al. and Lu et al.[4,17] The *iv* curve fit is differentiated (black line) and compared with the measured

DOI: 10.1021/am5083254
ACS Appl. Mater. Interfaces 2015, 7, 4039−4047

impedance (black dots) in accordance with eq 1. It is seen that the measured impedance followed the same trend, but that it was higher than expected based on the *iv* curve. The reason for this discrepancy is likely related to a chemically induced parasitic side reaction that becomes more pronounced at lower discharge rates. This will be discussed further in Section 4.1.

3.5. Charge at 250 μA. In Figure 6, we present typical EIS measurements during a charge. To limit the complexity of the analysis, impedance measurements are only made at voltages below 4.2 V to avoid the major decomposition reactions observed at higher potentials using DEMS. In this measurement, the 4.2 V limit corresponded to 60% SOC.

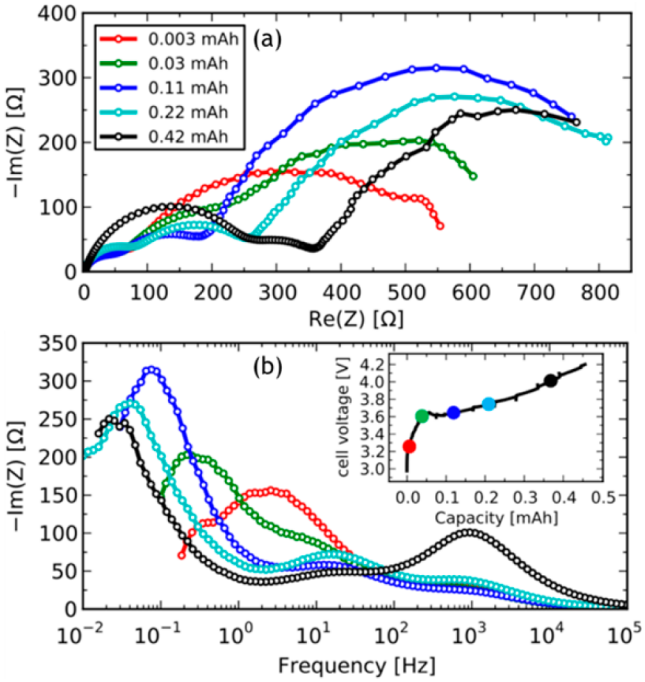

Figure 6. Nyquist (a) and Bode-like (b) plots of EIS measurements made during a 250 μA (220 μA/cm2) constant current charge. The charge followed a discharge similar to that shown in Figure 2 with a discharge resistance extrapolated to 3 kΩ at 2.0 V. The SOCs are shown as circles in the inset graph of the voltage profile. The 0.03 mAh and 0.42 mAh measurement was modeled using eq 3, and the obtained parameters are presented in Table 1

Three impedance contributions are identified. The correlation between the impedance and SOC is more complex than during discharge. The spectrum is dominated by a high- and a low-frequency response similar to Z_1 and Z_3 during discharge. It seems like the frequencies between 1 and 100 Hz are dominated by a mix of different processes appearing at certain SOCs and then disappearing at higher SOC, but further studies are needed to qualify this. The parameters obtained using equivalent circuit fitting on the green (0.03 mAh) and black (0.42 mAh) spectra with eq 3 are given in Table 1. The three contributions are in the same frequency ranges as seen during discharge. The polarization resistance, R_p, was almost constant in the range of 500−1000 Ω, but the peak frequencies and the relative magnitude of the different impedance contributions changed. Looking at the pseudocapacitances, C_1^* decreased from 3.6 μF to 0.6 μF, and C_3^* increased from 1.0 mF to 9.0 mF. This suggests that the active cathode area is increasing and that the active area of the anode is decreasing during charge. It is further noted that C_3^* is almost the same in the end of charge and in the beginning of the discharge (10.2 mF). Finally, it is noted that R_1 was almost constant until 3.7 V, after which it suddenly increased. This supports that the lithium anode surface is deactivated by an accelerated formation of the solid electrolyte interface (SEI) layer − possibly due to oxygen crossover.

4. DISCUSSION

To gain electrochemical knowledge of the fundamental reactions and bottlenecks during discharge and charge of the Li−O_2 battery, a series of electrochemical impedance spectra at different current densities and SOCs has been measured. It was seen that three impedance contributions were present during both discharge and charge, and they are referred to as Z_1, Z_2, and Z_3. The five key findings were that

(i) the impedance did not change at the discharge plateau,
(ii) Z_2 and Z_3 increased near sudden death,
(iii) C_3^* decreased significantly just before sudden death,
(iv) pseudocapacitances related to Z_1, Z_2, and Z_3 were typically 3 μF for C_1^*, 0.1−3 mF for C_2^*, and 1−20 mF for C_3^*, and
(v) the OCV was always 2.85 V during discharge and the initial stages of charge, then slowly increased to 3.2 V at the end of charge.

4.1. Identification of Processes during Discharge. Our results support previous findings by Adams et al. and Landa-Medrano et al. in refs 8 and 9 that Z_1 originates from the anode and that Z_2 and Z_3 originate from the cathode. In addition to this, our results show that Z_3 is a combination of the charge transfer reaction of oxygen reduction and the electronic transport through the Li_2O_2, whereas Z_2 is a cathode-specific process that is not related to the oxygen reduction. The assignment of anode and cathode features in the EIS is substantiated by the following three observations.

First, the full capacitance at the lithium anode surface is expected to be in the range of 10 μF as discussed in Section 2.2, whereas the capacitance of the XC72 electrode is expected to be 25 mF. If only part of an electrode is active during the EIS measurement, the capacitance will be lower. As reported, C_1^* was typically 3 μF, whereas C_2^* and C_3^* were in the range of 0.1−20 mF. Furthermore, the cathode capacitance per active surface area calculated by Adams et al. was in the same range as C_3^*.[8]

Second, the careful parameter study presented by Adams et al. in ref 8 shows that relevant cathode processes have peak frequencies below 10 Hz, which correspond with f_2 and f_3 in our study, whereas the peak frequency of the anode process is ∼1 kHz, which corresponds to f_1 in our study.

Third, Z_1 did not change during discharge, whereas Z_2 and Z_3 increased significantly close to sudden death. Both electrodes changed during the measurement. On the lithium anode, Younesi et al. have previously shown that an SEI layer is forming in a combination of chemical and electrochemical reactions,[33] but as shown by McCloskey et al. this is affecting neither the electrochemistry nor the measured impedance.[4] On the other hand, the cathode is covered with an insulating layer of mainly Li_2O_2 during discharge, and an increase in charge transfer resistance is typically captured in EIS measurements.

Ascribing Z_3 to oxygen reduction and electronic transport through Li_2O_2 is based on two observations: (i) Z_3 is the only process related to oxygen reduction, as both Z_1 and Z_2 are

DOI: 10.1021/am5083254
ACS Appl. Mater. Interfaces 2015, 7, 4039−4047

present in argon, and (ii) R_3 was the largest resistance during the entire discharge, both when the cathode was limited by reaction kinetics at the discharge plateau and by electronic conduction at sudden death.

The process related to Z_2 is cathode specific and not related to oxygen reduction, as it was present in argon but almost absent in a measurement with P50 carbon paper, shown in Figure S3 in the Supporting Information. As P50 is binder-free, this could indicate a degradation effect related to the PTFE binder. A little surprising, Z_2 was not present in the symmetrical cell measurement. This could indicate that the parasitic reaction was chemically passivated during handling when assembling the symmetrical cell.

The *iv* curve in Figure 5 was made to ensure that all electrochemical processes were captured in the impedance spectrum. This was indeed the case, since the total impedance could account for the changes in the overpotential. Actually, the measured impedance seemed to overestimate the slope of the *iv* curve, and the reason is most likely a result of lower Li_2O_2 formation yields, and therefore more heterogeneous discharge electrodeposits, at lower current densities as shown in a previous publication.[5] Garcia-Lastra et al. and Mekonnen et al. have shown that an increase of Li_2CO_3-like inclusions in the Li_2O_2 layer can change the electrical conductivity using DFT calculations,[34,35] and such changes would also change the current dependence of the impedance and explain the deviation.

4.2. Analysis of the Overpotential during Discharge. The measurements show that the electrochemistry was unchanged during the entire discharge, and they support the general understanding of tunneling being the dominant charge transport mechanism through the Li_2O_2 layer at relevant current densities and temperatures, which was initially proposed by Albertus et al.[16] and confirmed by Luntz et al.[1] Furthermore, the discharge was initially occurring in the entire cathode, whereas the increasing electronic transport through the growing Li_2O_2 layer passivated large parts of the cathode during discharge.

The tunneling mechanism is supported by two observations. First, the impedance contribution Z_3 related to oxygen reduction and electronic conduction through Li_2O_2 was constant at the discharge plateau and increased rapidly near sudden death, which is characteristic for the tunneling barrier that depends exponentially on the Li_2O_2 layer thickness, and second, the electrochemistry was unchanged during the discharge, as shown by a constant 2 e^-/O_2 process and identification of the same three processes in the impedance spectra at all SODs.

Passivation of the cathode is observed in the pseudocapacitance C_3^*. At 20 μA, the initial value is 21 mF. This is the expected value of the entire cathode, which means that Li_2O_2 deposition is occurring in the entire cathode. The decrease in stage 1, as defined in Figure 3, reflects Li_2O_2 formation, because the introduction of a dielectric material in a capacitor changes the capacitance. In stage 2, the decrease is significant, cannot be explained by the dielectric layer of Li_2O_2 alone, and must therefore reflect a reduction in active surface area. The cathode passivates when the critical thickness of Li_2O_2 is reached and tunneling is no longer possible. In stage 3, the available surface area is not sufficient to support the constant current, and the voltage drops to enable conduction through the blocked parts of the electrode. This is seen as an increase in cathode resistance. When fully discharged, the resistance is too large, and the current cannot be supported within the cutoff limit of 2.2 V. This is in full agreement with observations made by Luntz et al. using flat glassy carbon electrodes in electrolysis cells.[1]

Because of discussions in literature on the significance of oxygen diffusion in the electrolyte, it is worth mentioning that the sudden death is not due to pore clogging and increased oxygen diffusion resistance. In a typical discharge, the average thickness of Li_2O_2 is 0.5−1 nm based on the BET surface area of XC-72. This means that the porosity and Damköhler number are almost unchanged during the entire discharge, and as stated by Wang et al.,[29] such small changes will not give rise to the sudden death behavior.

4.3. Analysis of the Overpotential during Charge. The EIS measurements from the charge confirm that the electrical resistivity through Li_2O_2 decreases in charge mode as proposed by Luntz et al. using flat glassy carbon electrodes[1] and show that the voltage increase during charge is a mixed potential rather than an increase in internal resistance, as McCloskey et al. have also suggested based on modeling.[10]

The change in resistivity in charge mode is identified by comparing the impedance at the end of discharge with the resistance in the beginning of the charge. During charge, the polarization resistance was ∼500 Ω at a current of 250 μA (220 $\mu A/cm^2$), which is much lower than the extrapolated value of 3 kΩ at 2.0 V during discharge. Furthermore, the charge resistance had only little dependence on the discharge current and depth of discharge, which suggests that the charge is not limited by the same process as the discharge. Luntz et al. have previously explained this by a reduction of the tunneling barrier because of a change in the Fermi energy by experiments on flat glassy carbon electrodes in an electrolysis cell.[1]

The mixed potential is identified because the impedance was not increasing as the charging potential increased, which indicates a change of reaction mechanisms. As shown by DEMS and Li_2O_2 titration, the charging reaction is not a 2 e^-/O_2 process but rather a 2.5−3 e^-/O_2 process, and parasitic electrochemical reactions are thus present during the entire charge.[5,10,11,15] Keeping in mind that the OCV never exceeded 3.2 V during charge, and no significant resistance increase was seen in the impedance spectra, it suggests that a mixed potential between these competing electrochemical reactions was established during charge to support the high current.

These results contradict the theory proposed by Chen et al. suggesting that the increase in charge overpotential occurs because the Li_2O_2 closest to the electronically conducting part of the cathode oxidizes first.[7] If this was the case, an increase of the charge resistance of at least an order of magnitude would be expected to explain the voltage increase, but the resistance does not increase by more than a factor of 2. Furthermore, after discharging under alternating O_2 isotope atmospheres, Li_2O_2 oxidation was found to preferentially occur at the Li_2O_2/electrolyte interface over the Li_2O_2/cathode interface during the initial stages of charge, as shown in a previous publication.[14]

Interestingly, R_1 increased four times when the battery reached 4 V, and C_1^* decreased to 20%. This suggests significant anode degradation and is in line with previous work by Younesi et al. showing how the SEI layer changes on the lithium metal during charge of a Li−O_2 battery.[33] At this point it is not possible to determine whether this change is caused by degradation of the anode or an overlapping cathode process, but if the increase is because of anode degradation, this will be important to prevent in a commercial Li−O_2 battery.

DOI: 10.1021/am5083254
ACS Appl. Mater. Interfaces 2015, 7, 4039−4047

5. CONCLUSION

By measuring EIS spectra at different current densities and different SOCs it was possible to assign the three identified contributions to either the cathode or the anode. Only one of the two cathode processes depended on the presence of oxygen. This indicates that this contribution was related to the Li_2O_2 formation. The other contribution was cathode specific and may reflect a degradation reaction related to the PTFE binder.

During discharge, the rapid potential change near the end of discharge was due to an increase in polarization resistance, primarily related to the charge transport through the Li_2O_2. This supports previously published work by Luntz et al. in ref 1, which states that the electronic transport through Li_2O_2 at relevant current densities is governed by tunneling.

In the initial part of the charge, the impedance was low compared to the end of discharge at sudden death. This supports that the electronic conductivity is improved when changing to charge mode, which has also been shown in a previous work on smooth glassy carbon cathodes in an electrolysis cell.[1] During charge, the voltage increased significantly, whereas the resistance and OCV were almost unchanged, and DEMS measurements identified the presence of parasitic reactions. This suggests that the electrochemistry changed during charge and that the voltage increase was due to a mixed potential of parasitic reactions and Li_2O_2 oxidation, established to support a constant current.

■ ASSOCIATED CONTENT

Ⓢ Supporting Information

Schematic illustration of the test cell, equivalent circuit diagrams, and EIS measurements on modified systems that suppress different features in the EIS spectrum made to support the conclusions made in the article. These modifications are (1) using a symmetrical carbon−carbon cell and (2) using a cathode with a different type of carbon. This material is available free of charge via the Internet at http://pubs.acs.org.

■ AUTHOR INFORMATION

Corresponding Author

*E-mail: jhoj@topsoe.dk. Phone: (+45) 27292175. Fax: (+45) 45272999.

Present Address

⊥Bryan D. McCloskey: Department of Chemical and Biomolecular Engineering, University of California and Environmental Energy Technologies Division, Lawrence Berkeley National Laboratory, Berkeley, CA 94720, United States.

Notes

The authors declare no competing financial interest.

■ ACKNOWLEDGMENTS

The authors acknowledge support of this work from the ReLiable project (Project No. 11-116792) funded by the Danish Council for Strategic Research Program Commission on Sustainable Energy and Environment.

■ REFERENCES

(1) Luntz, A. C.; Viswanathan, V.; Voss, J.; Varley, J. B.; Speidel, A.; Nørskov, J. K.; Scheffler, R. Tunneling and Polaron Charge Transport Through Li_2O_2 in Li-O_2 Batteries. *J. Phys. Chem. Lett.* **2013**, *4*, 3494−3499.

(2) Hummelshøj, J. S.; Blomqvist, J.; Datta, S.; Vegge, T.; Rossmeisl, J.; Thygesen, K. S.; Luntz, A. C.; Jacobsen, K. W.; Nørskov, J. K. Communications: Elementary Oxygen Electrode Reactions in the Aprotic Li-Air Battery. *J. Chem. Phys.* **2010**, *132*, 071101−1−071101−4.

(3) Hummelshøj, J. S.; Luntz, A. C.; Nørskov, J. K. Theoretical Evidence for Low Kinetic Overpotentials in Li-O_2 Electrochemistry. *J. Chem. Phys.* **2013**, *138*, 034703−1−034703−12.

(4) Viswanathan, V.; Nørskov, J. K.; Speidel, A.; Scheffler, R.; Gowda, S. R.; Luntz, A. C. Li−O_2 Kinetic Overpotentials: Tafel Plots from Experiment and First-Principles Theory. *J. Phys. Chem. Lett.* **2013**, *4*, 556−560.

(5) McCloskey, B. D.; Valery, A.; Luntz, A. C.; Gowda, S. R.; Wallra, G. M.; Garcia, J. M.; Mori, T.; Krupp, L. E. Combining Accurate O_2 and Li_2O_2 Assays to Separate Discharge and Charge Stability Limitations in Nonaqueous Li-O_2 Batteries. *J. Phys. Chem. Lett.* **2013**, *4*, 2989−2993.

(6) Zhong, L.; Mitchell, R. R.; Liu, Y.; Gallant, B. M.; Thompson, C. V.; Huang, J. Y.; Mao, S. X.; Shao-Horn, Y. In Situ Transmission Electron Microscopy Observations of Electrochemical Oxidation of Li_2O_2. *Nano Lett.* **2013**, *13*, 2209−2214.

(7) Chen, Y.; Freunberger, S. A.; Peng, Z.; Fontaine, O.; Bruce, P. G. Charging a Li-O_2 Battery Using a Redox Mediator. *Nat. Chem.* **2013**, *5*, 489−494.

(8) Adams, J.; Karulkar, M.; Anandan, V. *J.* Evaluation and Electrochemical Analyses of Cathodes for Lithium-Air Batteries. *J. Power Sources* **2013**, *239*, 132−143.

(9) Landa-Medrano, I.; Ruiz de Larramendi, I.; Ortiz-Vitoriano, N.; Pinedo, R.; Ignacio Ruiz de Larramendi, J.; Rojo, T. In Situ Monitoring of Discharge/Charge Processes in Li-O_2 Batteries by Electrochemical Impedance Spectroscopy. *J. Power Sources* **2014**, *249*, 110−117.

(10) McCloskey, B. D.; Speidel, A.; Scheffler, R.; Miller, D.; Viswanathan, V.; Hummelshøj, J. S.; Nørskov, J. K.; Luntz, A. C. Twin Problems of Interfacial Carbonate Formation in Nonaqueous Li-O_2 Batteries. *J. Phys. Chem. Lett.* **2012**, *3*, 997−1001.

(11) McCloskey, B. D.; Bethune, D. S.; Shelby, R. M.; Girishkumar, G.; Luntz, A. C. Solvents' Critical Role in Nonaqueous Lithium-Oxygen Battery Electrochemistry. *J. Phys. Chem. Lett.* **2011**, *2*, 1161−1166.

(12) Gowda, S. R.; Brunet, A.; Wallraff, G. M.; McCloskey, B. D. Implications of CO_2 Contamination in Rechargeable Nonaqueous Li-O_2 Batteries. *J. Phys. Chem. Lett.* **2013**, *4*, 276−279.

(13) McCloskey, B. D.; Scheffler, R.; Speidel, A.; Bethune, D. S.; Shelby, R. M.; Luntz, A. C. On the Efficacy of Electrocatalysis in Nonaqueous Li-O_2 Batteries. *J. Am. Chem. Soc.* **2011**, *133*, 18038−18041.

(14) McCloskey, B. D.; Scheffler, R.; Speidel, A.; Girishkumar, G.; Luntz, A. C. On the Mechanism of Nonaqueous Li-O_2 Electrochemistry on C and Its Kinetic Overpotentials: Some Implications for Li-Air Batteries. *J. Phys. Chem. C* **2012**, *116*, 23897−23905.

(15) McCloskey, B. D.; Luntz, A. C.; Bethune, D. S.; Shelby, R. M.; Mori, T.; Scheffler, R.; Speidel, A.; Sherwood, M. Limitations in Rechargeability of Li-O_2 Batteries and Possible Origins. *J. Phys. Chem. Lett.* **2012**, *3*, 3043−3047.

(16) Albertus, P.; Girishkumar, G.; McCloskey, B. D.; Sánchez-Carrera, R. S.; Kozinsky, B.; Christensen, J.; Luntz, A. C. Identifying Capacity Limitations in the Li/Oxygen Battery Using Experiments and Modeling. *J. Electrochem. Soc.* **2011**, *158*, A343.

(17) Lu, Y.-C.; Gasteiger, H. A.; Shao-Horn, Y. Method Development to Evaluate the Oxygen Reduction Activity of High-Surface-Area Catalysts for Li-Air Batteries. *Electrochem. Solid-State Lett.* **2011**, *14*, A70−A74.

(18) Lasia, A. Impedance of Porous Electrodes. *J. Electroanal. Chem.* **1995**, *397*, 27−33.

(19) Hirschorn, B.; Orazem, M. E.; Tribollet, B.; Vivier, V.; Frateur, I.; Musiani, M. Determination of Effective Capacitance and Film Thickness from Constant-Phase-Element Parameters. *Electrochim. Acta* **2010**, *55*, 6218−6227.

(20) Graves, C. *RAVDAV Data Analysis Software,* Version 0.9.7.

DOI: 10.1021/am5083254
ACS Appl. Mater. Interfaces 2015, 7, 4039−4047

(21) Jamnik, J.; Maier, J. Generalised Equivalent Circuits for Mass and Charge Transport: Chemical Capacitance and Its Implications. *Phys. Chem. Chem. Phys.* **2001**, *3*, 1668−1678.
(22) Aurbach, D.; Weissman, I.; Zaban, A.; Chusid, O. Correlation Between Surface Chemistry, Morphology, Cycling Efficiency and Interfacial Properties of Li Electrodes in Solutions Containing Different Li Salts. *Electrochim. Acta* **1994**, *39*, 51−71.
(23) Aurbach, D.; Zaban, A.; Schechter, A.; Ein-eli, Y.; Zinigrad, E.; Markovsky, B. The Study of Electrolyte Solutions Based on Ethylene and Diethyl Carbonates for Rechargeable Li Batteries. I. Li Metal Anodes. *J. Electrochem. Soc.* **1995**, *142*, 2873−2882.
(24) Barbieri, O.; Hahn, M.; Herzog, a.; Kötz, R. Capacitance Limits of High Surface Area Activated Carbons for Double Layer Capacitors. *Carbon* **2005**, *43*, 1303−1310.
(25) Zoltowski, P. *J.* On the Electrical Capacitance of Interfaces Exhibiting Constant Phase Element Behaviour. *J. Electroanal. Chem.* **1998**, *443*, 149−154.
(26) Gerbig, O.; Merkle, R.; Maier, J. Electron and Ion Transport in Li_2O_2. *Adv. Mater.* **2013**, *25*, 3129−3133.
(27) Dunst, A.; Epp, V.; Hanzu, I.; Freunberger, S. A.; Wilkening, M. Short-Range Li Diffusion vs. Long-Range Ionic Conduction in Nanocrystalline Lithium Peroxide Li_2O_2 - the Discharge Product in Lithium-Air Batteries. *Energy Environ. Sci.* **2014**, *7*, 2739−2752.
(28) Young, K. F.; Frederikse, H. P. R. Compilation of the Static Dielectric Constant of Inorganic Solids. *J. Phys. Chem. Ref. Data* **1973**, *2*, 313.
(29) Wang, Y.; Cho, S. C. Analysis of Air Cathode Perfomance for Lithium-Air Batteries. *J. Electrochem. Soc.* **2013**, *160*, A1847−A1855.
(30) Mehta, M.; Mixon, G.; Zheng, J. . P.; Andrei, P. Analytical Electrochemical Impedance Modeling of Li-Air Batteries under D.C. Discharge. *J. Electrochem. Soc.* **2013**, *160*, A2033−A2045.
(31) Sandhu, S. S.; Fellner, J. P.; Brutchen, G. W. Diffusion-Limited Model for a Lithium/Air Battery with an Organic Electrolyte. *J. Power Sources* **2007**, *164*, 365−371.
(32) Schiller, C. A.; Richter, F.; Gülzow, E.; Wagner, N. Validation and Evaluation of Electrochemical Impedance Spectra of Systems with States that Change with Time. *Phys. Chem. Chem. Phys.* **2001**, *3*, 374−378.
(33) Younesi, R.; Hahlin, M.; Roberts, M.; Edström, K. The SEI Layer Formed on Lithium Metal in the Presence of Oxygen: A Seldom Considered Component in the Development of the Li-O_2 Battery. *J. Power Sources* **2013**, *225*, 40−45.
(34) Garcia-Lastra, J. M.; Myrdal, J. S. G.; Christensen, R.; Thygesen, K. S.; Vegge, T. DFT+U Study of Polaronic Conduction in Li_2O_2 and Li_2CO_3: Implications for Li-Air Batteries. *J. Phys. Chem. C* **2013**, *117*, 5568−5577.
(35) Mekonnen, Y. S.; Knudsen, K. B.; Mýrdal, J. S. G.; Younesi, R.; Højberg, J.; Hjelm, J.; Norby, P.; Vegge, T. Communication: The Influence of CO_2 Poisoning on Overvoltages and Discharge Capacity in Non-aqueous Li-Air Batteries. *J. Chem. Phys.* **2014**, *140*, 121101.

DOI: 10.1021/am5083254
ACS Appl. Mater. Interfaces 2015, 7, 4039−4047